Available online at www.sciencedirect.com
ScienceDirect
International Journal of Impact Engineering 34 (2007) 859–873
INTERNATIONAL JOURNAL OF IMPACT ENGINEERING
www.elsevier.com/locate/ijimpeng

Scaling the response of circular plates subjected to large and close-range spherical explosions. Part I: Air-blast loading

A. Neuberger[a,b,*], S. Peles[c], D. Rittel[a]

[a]*Technion, Faculty of Mechanical Engineering, Israel Institute of Technology, 32000 Haifa, Israel*
[b]*MOD, Tank Program Management, Hakirya, Tel-Aviv, Israel*
[c]*IMI, Central Laboratory Division, Ramat Hasharon, P.O. Box 1044, Israel*

Received 5 January 2006; accepted 9 April 2006
Available online 12 June 2006

Abstract

This two-part paper addresses scaling of the dynamic response of clamped circular plates subjected to close-range and large spherical blast loadings.

Full-scale experiments involving actual geometries and charges are quite involved and costly, both in terms of preparation and measurements. For these reasons, scaled-down experiments are highly desirable. However, the validity of such experiments remains to be firmly established, and this is the main objective of this paper.

In this study, similarity is obtained by using replica scaling for all geometrical parameters, while the blast effect is scaled by using the well-known Hopkinson scaling law. We also consider the overall effect of the strain rate sensitivity and variability of material properties with plate thickness on the response of the scaled model.

This study presents numerical and experimental results from a series of controlled explosion experiments. The first part of the paper deals with spherical charges exploding in *free air*, while the second part deals with the same charges *flush buried* in dry sand. A good agreement between numerical simulation predictions and test results was obtained, so that the main result of the two papers is that scaling can be successfully applied to assess the dynamic response of armor plates subjected to close-range large explosions.

Keywords: Close-range; Large blast; Dynamic response; Circular plate; Scaling

1. Introduction

Understanding the dynamic behavior of blast loaded armor steel plates is a key to successful protection projects. The literature on blast loaded plates is quite abundant. Numerous studies of experimental and/or numerical nature have been carried out and reported (see, e.g. [1–9]). These studies characterize the different failure modes and the relationship between deformation and tearing of clamped blast loaded plates. The failure modes were first defined by Menkes and Opat [10] for the case of impulsively loaded clamped beams.

*Corresponding author. MOD, MANTAK, Tank Program Management, Hakirya, Tel-Aviv, Israel.
E-mail address: navidov@gmail.com (A. Neuberger).

0734-743X/$ - see front matter © 2006 Elsevier Ltd. All rights reserved.
doi:10.1016/j.ijimpeng.2006.04.001

Nomenclature

A	Johnson–Cook (J–C) coefficient
B	J–C coefficient
C	J–C coefficient
C_i	polynomial coefficients
D	plate diameter
I	impulse
m	J–C coefficient
n	J–C coefficient
P	blast pressure
R	distance from center of spherical charge
S	scaling factor
t	plate thickness
T	temperature
V	relative volume of the gas products to the initial explosive state
W	charge weight
Z	scaled distance
E	energy
δ	peak deflection
$\varepsilon, \dot{\varepsilon}$	strain, strain rate
θ	angle of incidence
ρ	material density
σ	stress
τ	time
ζ	scaled impulse
Π	characteristic similarity parameter

The classification was as follows: mode I for large inelastic deformation, mode II for tearing at the support, and mode III for shear failure at the support. These failure modes were also adopted for blast loaded circular plates, and further subdivisions were observed and defined by other authors. In contrast to the large number of studies mentioned previously, the literature on scaling (similarity) of the structural response is quite sparse. Wen and Jones [11] investigated the scaling of metal plates subjected to impact and concluded that geometrical scaling can be applied. These authors also reported that strain rate sensitivity does not significantly affect scaling for their experiments. Jacob et al. [12] investigated scaling aspects of quadrangular plates subjected to localized blast loads. The effects of varying the charges' weight and plate geometries on the deformation were described and analyzed. Furthermore, a modified dimensionless number was introduced to represent the quadrangular plate's response to a localized disc charge. The validity of the presented results is limited to the investigated small plate geometries and loading conditions, while numerical simulations and experiments for larger explosions are still required.

Raftenberg presented a study on close-range small blast loading on a steel disc [13]. This study compared experimental data to several numerical finite elements calculations, based on different constitutive models in order to validate specific dynamic material parameters. The Johnson–Cook model for RHA steel was found to produce results in reasonable agreement with experiments for the problem at hand. Hanssen et al. [14] investigated the behavior of aluminum foam panels subjected to close-range blast loading. This study addressed the performance of additional sacrificial layers as a protecting layer. However, it was observed that the energy and impulse transfer to the protected structure was not reduced by adding a sacrificial foam panel, but contrary to the expectations, the impulse increased due to the proximity of the explosion.

The combination of *scale modeling* of the dynamic response of a plate subjected to a very *large explosion* from a *close-range* was not studied yet, to the best of the authors' knowledge.

Therefore, these papers present scaling aspects of the quantities that characterize the dynamic response of a plate subjected to close-range large blasts. Part I of the study reports finite elements simulations and experiments of blast loaded circular plates subjected to explosions in free air. The numerical calculations and the tests were conducted on different scale factors S (where $S = 2$ refers to one-half scaling), where the reference plate ($S = 1$) is 0.05 m thick with a 2 m diameter. Part II of the study addresses the effects of sand-buried charges. The main outcome of the two papers is that scaling can be applied to analyze armor plates subjected to close-range large air blasts as well as buried charges. This study also shows that the variation of mechanical properties with plate thickness affects the similarity result and should therefore be taken into account.

The paper is organized as follows: Section 2 presents elements of the physical similarity and scale modeling used in this work, followed by Section 3 that details the numerical approach. Section 4 describes the test setup and measuring technique, while Section 5 presents the numerical results, followed by the experimental results. Section 6 discusses the key points of the study, followed by concluding remarks.

2. Elements of scaling theory

The validation of physical similarity of a specific phenomenon is crucial for proper scaling. Before a large scale *prototype* is built, experiments on a small scale *model* are required. However, one must know how to scale the model experimental results up to the full scale prototype. The concept of physical similarity was stated by Barenblatt [15] as a natural generalization of similarity in geometry, so that '*physical phenomena are called similar if they differ only in respect of the numerical values of the dimensional governing parameters while the values of the corresponding dimensionless parameters (Π-terms) being identical*'. The objective is to obtain identical relationships between quantities that characterize both, the *prototype*, regarding the original size, and the *model*, regarding the scaled-down phenomena.

The principles of scaling and the relationships between the small scale model parameters and the full-scale prototype parameters were stated by Jones [16]. Here we will present the relevant parameters for the investigated problem in terms of proportion between the *prototype* parameter (superscripts P) and the corresponding *model* parameter (superscripts M), as follows:

- Linear dimensions are proportional to the scale factor, $x_i^{\mathrm{P}} = x_i^{\mathrm{M}} \cdot S$.
- Angles are the same, $\alpha_i^{\mathrm{P}} = \alpha_i^{\mathrm{M}}$.
- Densities of materials are the same, $\rho_i^{\mathrm{P}} = \rho_i^{\mathrm{M}}$.
- Stresses of each material are the same, $\sigma_i^{\mathrm{P}} = \sigma_i^{\mathrm{M}}$.
- Characteristic times are proportional to the scale factor, $\tau_i^{\mathrm{P}} = \tau_i^{\mathrm{M}} \cdot S$.
- Strains are identical, $\varepsilon_i^{\mathrm{P}} = \varepsilon_i^{\mathrm{M}}$.
- Loads are the same, and must act at scaled locations, $F_i^{\mathrm{P}} = F_i^{\mathrm{M}}$ at $x_i^{\mathrm{P}} = x_i^{\mathrm{M}} \cdot S$.
- Deformations at geometrically scaled locations for corresponding scaled times are proportional to the scale factor, $\delta_i^{\mathrm{P}} = \delta_i^{\mathrm{M}} \cdot S$ at $\tau_i^{\mathrm{P}} = \tau_i^{\mathrm{M}} \cdot S$.
- Angular deformations are the same, $\omega_i^{\mathrm{P}} = \omega_i^{\mathrm{M}}$.

It should be noted that several phenomena may not scale according to these principles. For example gravitational forces cannot be scaled according to the basic principles of geometrically similar scaling. However, here high accelerations are involved therefore the gravitational forces are not significant and can thus be neglected. Strain rate sensitivity in a small-scale model is scale factor times larger than that in a geometrically similar full-scale prototype. For the case at hand, considering the actual strain rates produced during the dynamic bulging process, the material properties are taken to be approximately scale-independent. Finally, fracture cannot be scaled according to the basic principles of geometrically similar scaling. However, fracture is beyond the scope of the present work.

When scaling spherical blast wave phenomena, the most common scaling method is Hopkinson, or ''cube root'' scaling law as shown by Baker [17]. This scaling law states that self-similar blast waves are produced at

identical scaled distances when two explosive charges of similar geometries and explosive, but of different weight, are detonated in the same atmosphere. For explosions in air, the Hopkinson scaled parameters are [17]:

$$Z = \frac{R}{E^{1/3}}, \quad \tau^* = \frac{\tau}{E^{1/3}}, \quad \zeta = \frac{I}{E^{1/3}}, \tag{1}$$

where Z is the scaled distance, τ^* is the characteristic scaled time of the blast wave, ζ is the scaled impulse, R is the distance from center of blast source, and E is the source blast energy. This law implies that all quantities with dimension of pressure and velocity are unchanged through scaling, i.e. for the same value of Z (note that E can be replaced by the blast source weight W). In this study, Hopkinson's method was used to calculate the corresponding charge weight for the scaled down model as follows:

$$W^{\mathrm{M}} = W^{\mathrm{P}}/S^3. \tag{2}$$

3. Numerical simulations

The numerical simulations were carried out using LS-DYNA finite element code [18]. The software has the ability to simulate dynamic structural response in several ways, including pure Lagrangian, and coupled Lagrange–Eulerian methods. The purely Lagrangian approach combined with a simplified engineering blast model is more desirable since it reduces the calculation time. However, both methods were used and compared with the experimental data. The multi-material Eulerian formulation is part of the Arbitrary-Lagrangian–Eulerian (ALE) solver within LS-DYNA. By combining the ALE solver with an Eulerian–Lagrangian coupling algorithm, a structural or Lagrangian mesh can interact with the gas products or Eulerian mesh. This technique was used for the ranges where the simplified blast model produced uncertain impulse duration as a result of blast proximity.

3.1. Simplified blast model

'Load-blast' boundary condition, which is implemented in LS-DYNA, was used to load the tested circular plate with the appropriate varying pressure distribution. This function is based on an implementation by Randors-Pehrson and Bannister (1997) of the empirical blast loading functions by Kingery and Bulmash [19] that were implemented in the US Army Technical Manual ConWep code [20].

The blast loading equation is stated as follows:

$$P(\tau) = P_{\mathrm{r}} \cdot \cos^2\theta + P_{\mathrm{i}} \cdot (1 + \cos^2\theta - 2\cos\theta), \tag{3}$$

where θ is the angle of incidence, defined by the tangent to the wave front and the target's surface, P_{r} is the reflected pressure, and P_{i} is the incident pressure. This blast function can be used for the following two cases: free air detonation of a spherical charge, and ground surface detonation of a hemispherical charge. To calculate the pressure over certain predefined group of surfaces related to the geometry of the analyzed structure, the model uses the following inputs: equivalent weight of TNT explosive, the spatial coordinate of the detonation point, and the type of blast (spherical or hemispherical). The actual impulse, I, corresponding to the charge's weight and distance to the target, can be derived from the ConWep database [20] that is implemented into the 'load-blast' function of LS-DYNA software. For example, considering the problem analyzed here, the spherical TNT charge's weight is $W = 50\,\mathrm{kg}$, and the distance from the target is $R = 0.5\,\mathrm{m}$. Then, the impulses are $I(\mathrm{incident}) = 1563\,\mathrm{kPa\,ms}$, and $I(\mathrm{reflected}) = 45{,}220\,\mathrm{kPa\,ms}$.

Note that the model accounts for the angle of incidence of the blast wave, but it does not account for shadowing by intervening objects or for the confinement effects, causing the blast to focus on a certain zone.

3.2. Material behavior

The ALE model involves three different material types. The first material model represents the rolled homogeneous armor (RHA) steel plate, followed by the TNT spherical explosive charge, and finally the

surrounding air media, which is used to fill the space affected by the explosive charge. Note that in the purely Lagrangian approach, only one type of material model is needed, namely for the steel plate.

The circular steel plate is represented by a finite element mesh created by FEM-PATRAN preprocessor software. By using the inherent symmetry of the studied problem calculation time can be saved. Thus, only a quarter of the circular plate was modeled with the appropriate boundary conditions applied along the symmetry planes as shown in Fig. 1. The entire model was constructed from constant stress hexagonal solid elements formulation with one integration point.

To represent the dynamic mechanical behavior of the RHA steel two constitutive material models were compared. The first model represents a strain rate insensitive bilinear material. The second model represents a strain rate sensitive material, represented by the Johnson–Cook (J–C) constitutive model [21]. The J–C model is stated as follows:

$$\sigma_y = \left(A + B \cdot \bar{\varepsilon}_{\mathrm{p}}^{n}\right) \cdot (1 + c \cdot \ln \dot{\varepsilon}^*) \cdot (1 - T^m), \tag{4}$$

where A, B, c, n and m are the J–C material coefficients, as listed in Table 1 [20,21], ε_{p} is the effective plastic strain, $\dot{\varepsilon}^* = \dot{\bar{\varepsilon}}^{\mathrm{p}}/\dot{\varepsilon}_0$ is the effective plastic strain rate at a reference strain rate $\dot{\varepsilon}_0 = 1\,\mathrm{s}^{-1}$, and the homologous temperature $T = (T' - T'_{\mathrm{room}})/(T'_{\mathrm{melt}} - T'_{\mathrm{room}})$ where T' is the material's temperature, T'_{room} is the room temperature, and T'_{melt} is the material's melting temperature.

The J–C constitutive material model is incorporated with a polynomial equation of state which is linear in internal energy E. The pressure P is given by

$$P = C_0 + C_1\mu + C_2\mu^2 + C_3\mu^3 + (C_4 + C_5\mu + C_6\mu^2)E, \tag{5}$$

where the terms $C_2\mu^2$ and $C_6\mu^2$ are set to zero if $\mu = (\rho/\rho_0) - 1 < 0$, and ρ/ρ_0 is the ratio of the current to initial density.

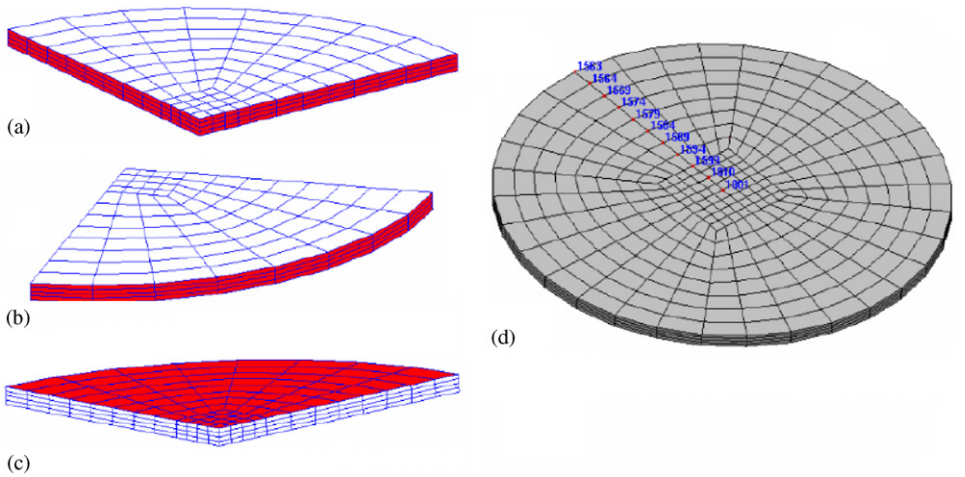

Fig. 1. Finite elements model: (a) symmetry B.C.; (b) constrained B.C.; (c) 'load-blast' B.C.; (d) entire model including measurement points.

Table 1
RHA class 1 mechanical properties and the corresponding Johnson–Cook coefficients [24]

t (mm)	σ_y (MPa)	σ_{UTS} (MPa)	ε_{L} (%)	E (GPa)	v	Hardness (HBW)	A (MPa)	B (MPa)	n	c	m
3–20	950	1250	9			380–430	950	560			
21–40	900	1150	10	210	0.28	340–390	900	545	0.26	0.014	1
41–80	850	1050	11			300–350	850	355			

The TNT explosive charge was modeled via Jones–Wilkins–Lee (JWL) equation of state (EOS) for explosive detonation products [22]. The pressure field is given by

$$P = A\left(1 - \frac{\omega}{R_1 V}\right)e^{-R_1 V} + B\left(1 - \frac{\omega}{R_2 V}\right)e^{-R_2 V} + \frac{\omega E'}{V}, \tag{6}$$

where A, B, C, R_1, R_2, and ω are constants that can be found in the literature [23], $V = v/v_0$ is the relative volume of the gas products to the initial explosive state, and E' is the energy per unit volume.

The medium in which the blast wave propagates (air) was modeled with a linear polynomial EOS for linear internal energy, which is given by

$$P = C_0 + C_1 m + C_2 m^2 + C_3 m^3 + \left(C_4 + C_5 m + C_6 m^2\right)E^*, \tag{7}$$

where $m = \rho/\rho_0 - 1$ with ρ/ρ_0 being the ratio of the current to initial density, $C_{1,\ldots,6}$ are polynomial coefficients, and E^* has units of pressure. To model gases, the gamma law EOS can be used. This implies that $C_0 = C_1 = C_2 = C_3 = C_6 = 0$ and $C_4 = C_5 = \gamma - 1$, where γ is the ratio of specific heats. Therefore Eq. (7) becomes

$$P = (\gamma - 1)\frac{\rho}{\rho_0}E^*. \tag{8}$$

4. Test setup

Two different scaled-down similar test rigs (of scale-down factors $S = 2$ and 4) were built in order to experimentally assess the applicability of scale-down modeling of the studied problem. The experimental test setup of each structure is shown in Fig. 2. The target plate was supported by two thick armor steel plates with circular holes that were tightened together with bolts and clamps. The thick plate that faces the charge has a hole with inclined side walls to prevent reflection of the blast wave to the tested plate as shown schematically in Fig. 3.

The measurement of the maximum dynamic deflection of the plate was achieved by means of a specially devised comb-like device. The teeth of the comb possess a gradually decreasing height, as shown in Fig. 4. When positioned under the dynamically deflecting plate, the long teeth are permanently bent while those that are shorter than the maximum deflection remain intact. Therefore, a direct estimation of the maximum deflection is immediately available after the blast test. We found that this inexpensive device provides a sufficiently accurate measure of the dynamic deflection. Note that the accuracy of the measurement is related to the height difference between the teeth.

The spherical TNT charges were hanged in air using fisherman's net and were ignited from the center of the charge.

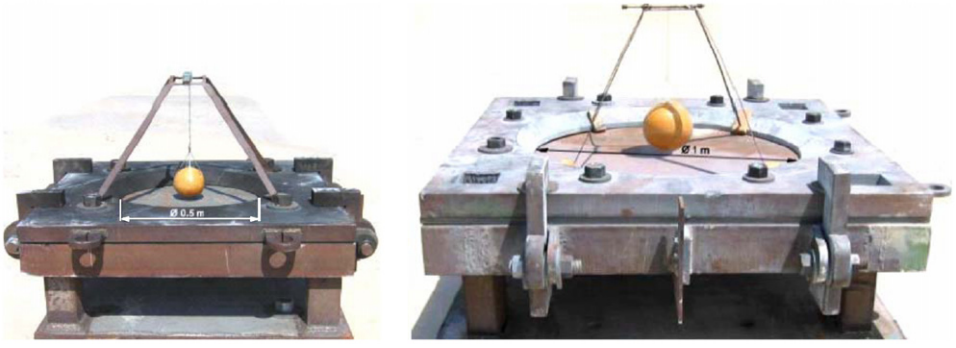

Fig. 2. Experimental setup at 2 different scales ($S = 4$, left, and $S = 2$, right)

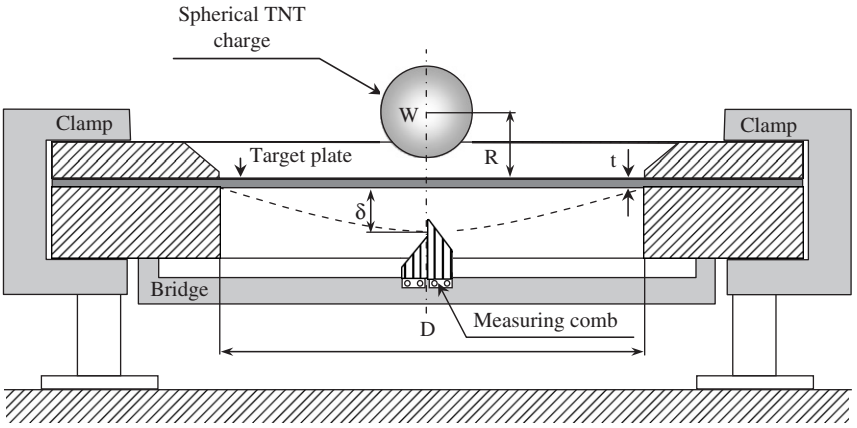

Fig. 3. Schematic drawing of the test rig and the measurement setup.

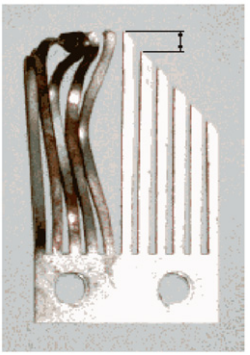

Fig. 4. Comb-like device for dynamic deflection measurement.

5. Results

5.1. Numerical results

The numerical calculations comprised 4 distinct stages, and the same problem was calculated each time at different scale factors, namely $S = 1$, 2, 4, 10, and 0.5.

The first stage deals with the boundary conditions and their influence on the deflection profile of the plate. Three different boundary conditions were investigated: 'free', 'constrained' (or clamped), and a characteristic 'structure' as shown in Fig. 5. The characteristic structure enables us to analyze the effect of supporting side walls on the dynamic response of the plate. The objective of this preliminary study was to investigate the differences between the three dynamic responses and select the most appropriate boundary conditions for the following calculations.

The second stage involves selection of a simple rate-insensitive bilinear material model and calculation of the deflections and stresses at different scaling factors. Here the objective is to explore scalability of the dynamic response with "ideal" parameters.

The third stage introduces rate-sensitivity of the mechanical properties of the steel plate through the Johnson–Cook model [21]. The objective of this stage is to study the effect of the strain rate sensitivity on the dynamic response at different scale factors for the problem at hand.

Finally, stage 4 addresses variability of the material properties with the rolled plate thickness as a result of the manufacturing process. This stage was carried out at three different scale factors. The results of each stage will now be presented and discussed.

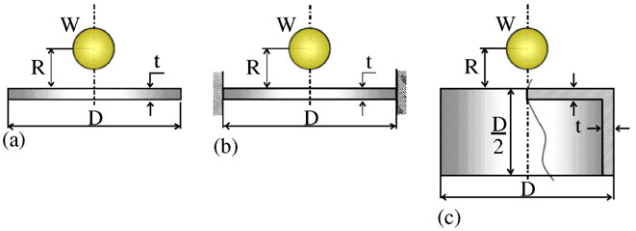

Fig. 5. Comparison between different boundary conditions: (a) free, (b) constrained; (c) structure.

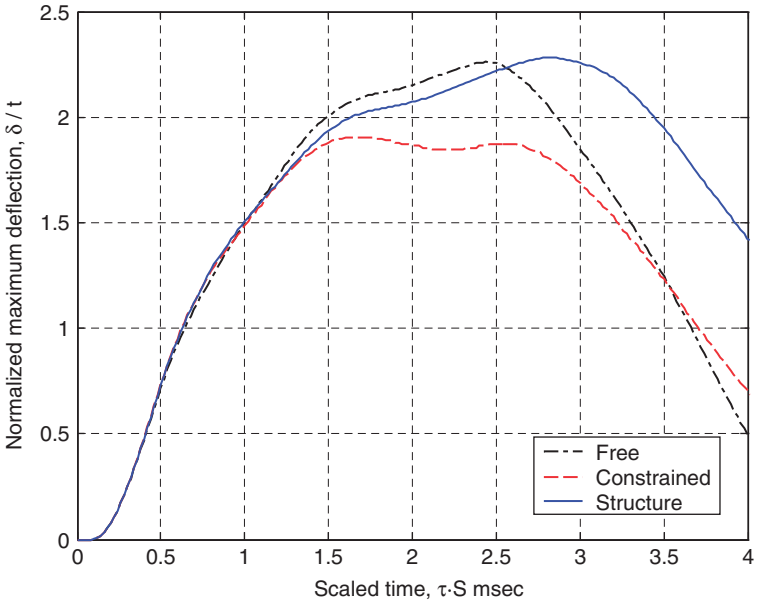

Fig. 6. Midpoint normalized deflection vs. scaled time for free, constrained, and structure boundary conditions.

5.1.1. Stage 1: influence of the boundary conditions

The effect of the three different boundary conditions on the dynamic response (i.e. deflection–time history) at the midpoint of the plate is shown in Fig. 6. The following parameters were taken: plate thickness $t = 0.05$ m, plate diameter $D = 2$ m, charge's weight $W = 50$ kg TNT, and distance from the plate's surface to the center of the charge $R = 0.5$ m. The RHA class 1 material properties were represented via bilinear model with the following parameters: yield strength $\sigma_y = 1000$ MPa, Young's modulus $E = 210$ GPa, and hardening plastic modulus $E_p = 2$ GPa. The deflection at the midpoint of the plate is calculated as the difference between the midpoint and the circumference vertical displacements. Fig. 6 shows the deflection time history of the blast loaded plate for each type of boundary condition. It can be seen that the peak deflection occurs at scaled times of the order of ~2 ms. The 'free' and 'structure' types of boundary conditions produce relatively equal peak deflections while the 'constrained' type has a peak deflection which is approximately 20% smaller than the others. Furthermore, even though the 'free' and 'structure' boundary conditions are quite similar in their peak deflection, it can be seen that they yield a different duration of the bulging process, where the deflection in the 'structure' boundary condition lasts longer than in the 'free' type as a result of the added inertia of the side walls. From this point further on, we applied the 'constrained' boundary conditions only, since they were found to be closer to the actual experimental boundary conditions.

5.1.2. Stage 2: scaling with bilinear material model

The objective of the second stage is to validate the scale modeling using the combined Hopkinson-Replica method for ideal material properties of the blast loaded plate, namely bilinear material properties as shown

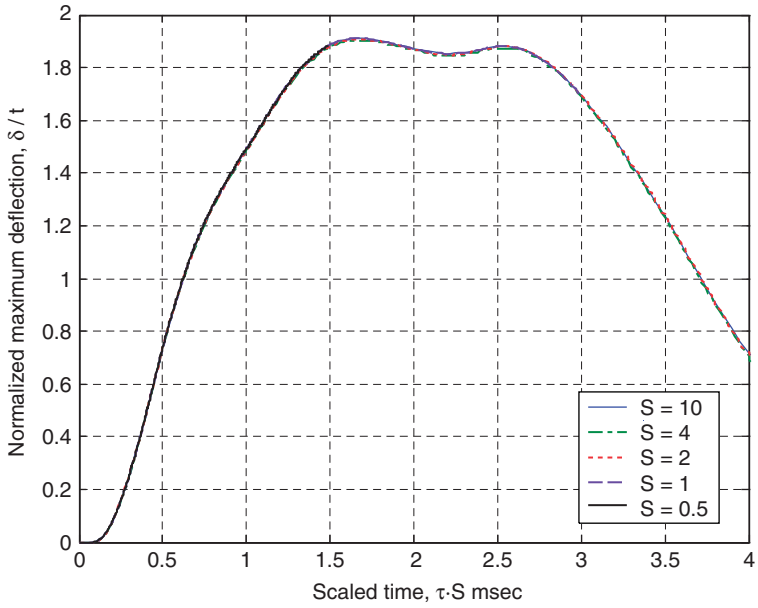

Fig. 7. Normalized midpoint deflection vs. scaled time at different scales (bilinear material model).

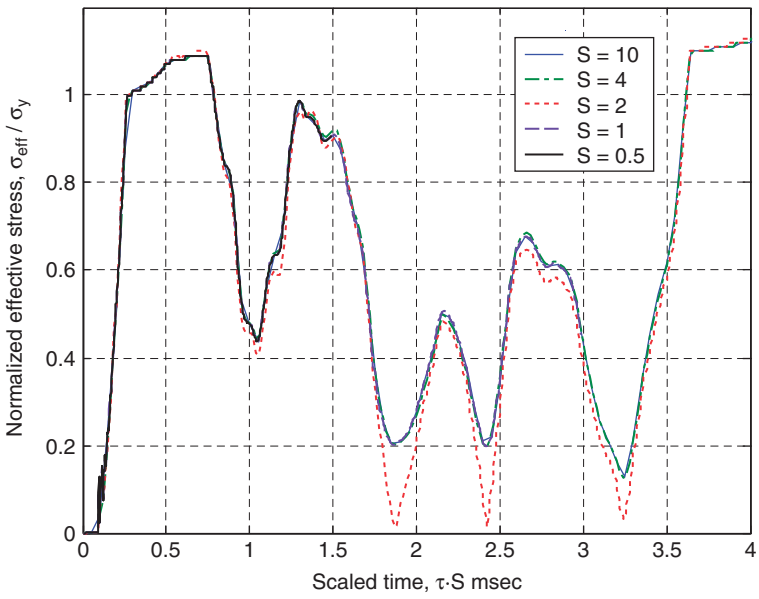

Fig. 8. Normalized stresses vs. scaled time at different scales (bilinear material model).

previously. Fig. 7 shows the normalized midpoint deflection scaled time history at various scaling factors ranging from $S = 0.5$ to 10. The plate thickness at scale factor $S = 1$ is $t = 0.05$ m, plate diameter $D = 2$ m, charge weight $W = 50$ kg TNT, and the distance from center of charge $R = 0.5$ m. This is equivalent to selecting a scaling factor of $S = 4$ for instance, so that $t = 0.0125$ m, $D = 0.5$ m, and $R = 0.125$ m. In that case the corresponding charge is scaled down to $W = 0.781$ kg TNT. This figure shows that all the curves merge together, showing an excellent scaling of the plates midpoint deflection. It should be mentioned that the same procedure was applied for different "measurement" points on the plate (Fig. 1) at all scaling factors, and identical results were obtained. Fig. 8 shows the scaled time history of the normalized stresses at the midpoint

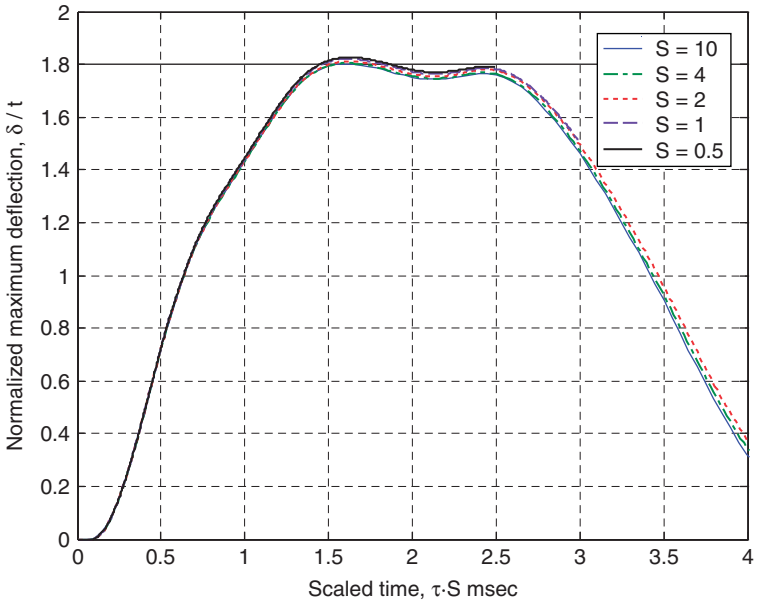

Fig. 9. Normalized midpoint deflection vs. scaled time at different scales (Johnson–Cook constitutive model).

of the plate for the corresponding conditions shown above. One should again emphasize that the material is considered as rate-insensitive in these calculations.

5.1.3. Stage 3: scaling with strain-rate sensitive material model (J–C)

The objective of the third stage is to assess the influence of the material's strain-rate sensitivity on the scale modeling of blast loaded plate. Here, the steel plate was modeled using Johnson–Cook model [21] with the following coefficients: $A = 1000\,\text{MPa}$, $B = 500\,\text{MPa}$, $c = 0.014$, $n = 0.26$, and $m = 1$. Fig. 9 shows the normalized midpoint deflection scaled time history for various scaling factors. Here too, it can be seen that all the curves merge almost perfectly to a single curve, thus showing excellent scaling of the problem. The numerical calculations show that for $S = 1$, the strain rate at the maximum deflected elements is of the order of $\dot{\varepsilon}_{S=1} \approx 200\,\text{s}^{-1}$, whereas for $S = 10$, it reaches $\dot{\varepsilon}_{S=10} \approx 1000\,\text{s}^{-1}$. In this range of strain rates, the Johnson–Cook model [21] predicts a very small change in the yield or flow stress. Therefore, one may conclude that, given the actual strain rates produced during the dynamic bulging process, strain-rate sensitivity has a negligible effect on the scalability of the problem at hand, for the range of scaling factors investigated here. However, this may not always be the case when highly strain rate sensitive materials are considered.

5.1.4. Stage 4: scaling with material properties variability with thickness (J–C)

The objective of this stage is to assess the extent to which a certain variability of the mechanical properties of the rolled plate, for each plate's thickness, may affect the validity of the present scaling procedures. To be more specific, let us consider the RHA class 1 armor steel material. Due to manufacturing limitations its properties vary with the thickness, as shown in Table 1. For example, a plate of $t = 0.01\,\text{m}$ thickness has a yield strength $\sigma_y = 950\,\text{MPa}$ and UTS strength $\sigma_{UTS} = 1250\,\text{MPa}$. When the thickness becomes $t = 0.04\,\text{m}$ the corresponding material properties are reduced to following values: yield strength $\sigma_y = 850\,\text{MPa}$ and UTS strength $\sigma_{UTS} = 1050\,\text{MPa}$ [24]. The corresponding Johnson–Cook coefficients in this table were taken as follows: A is the yield strength of the material, B is calculated to obtain the UTS strength at the given maximum elongation, while n, c, and m remain unaffected and can be found in literature [21]. This investigation was performed at three different scale factors $S = 1$, 2, and 4 for the same problem as before. The simulations results are shown in Figs. 10 and 11, where the differences between the dynamic responses at each of the three scale factors are shown. In order to further study the influence of the material properties, larger plastic strains were investigated. This was achieved by modeling a thinner plate and a larger charge from

closer range as follows: at scale factor $S = 1$ the plate thickness is $t = 0.04$ m, plate diameter $D = 2$ m, charge weight $W = 70$ kg TNT, and the distance from center of charge $R = 0.26$ m. Fig. 12 shows the normalized midpoint deflection scaled time history at the three scaling factors $S = 1$, 2, and 4. It can be seen that, due to the difference between the material properties for each material thickness, the resulting curves of each scale factor diverge from each other to approximately ~7% peak deflection, starting with scale factor $S = 1$ up to scale factor $S = 4$. Therefore, scale modeling of the present problem is distorted, so that the deviation should be taken into account when scaling the results from the model up to the prototype. Fig. 13 shows the scaled

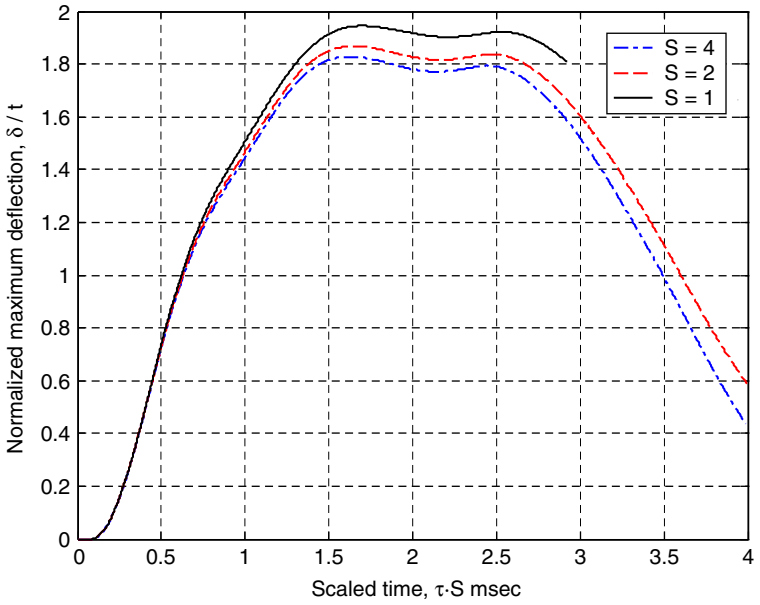

Fig. 10. Normalized deflection at different scales vs. scaled time (material properties vary with thickness).

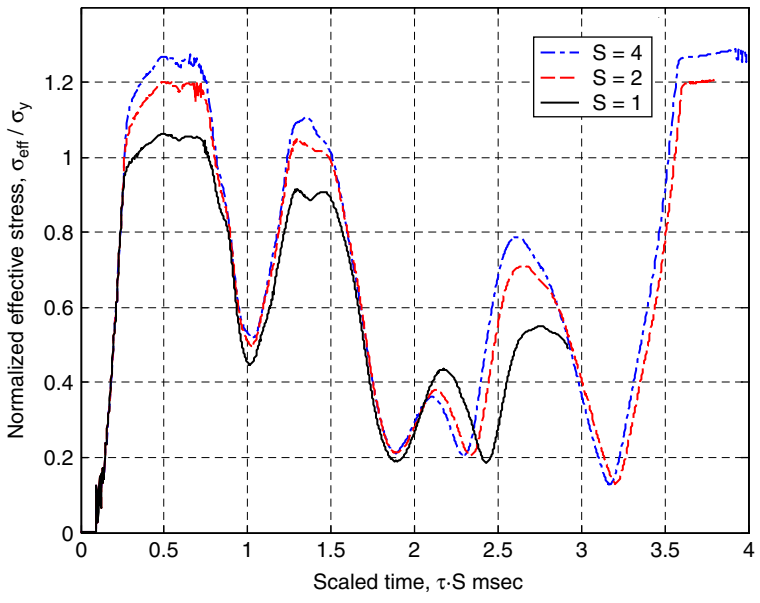

Fig. 11. Normalized effective stress at different scales vs. scaled time (material properties vary with thickness).

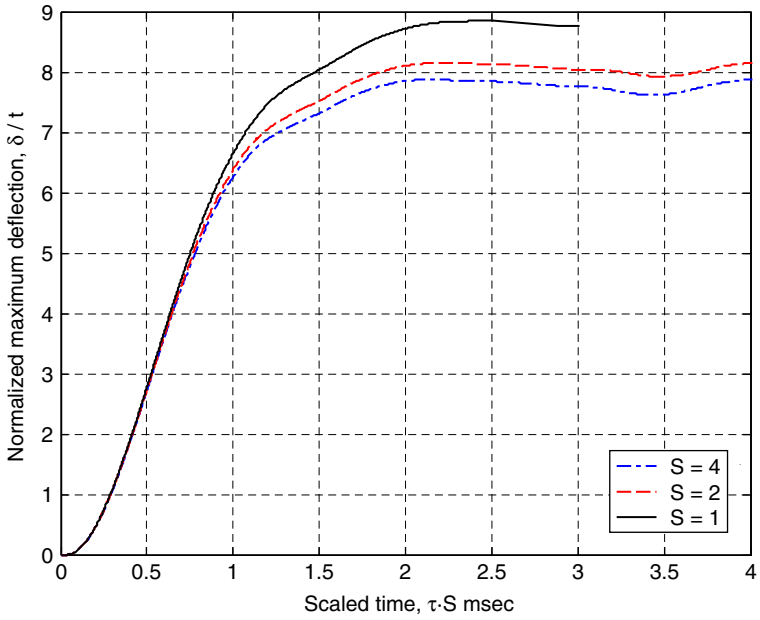

Fig. 12. Normalized deflection at different scales vs. scaled time (material properties vary with thickness).

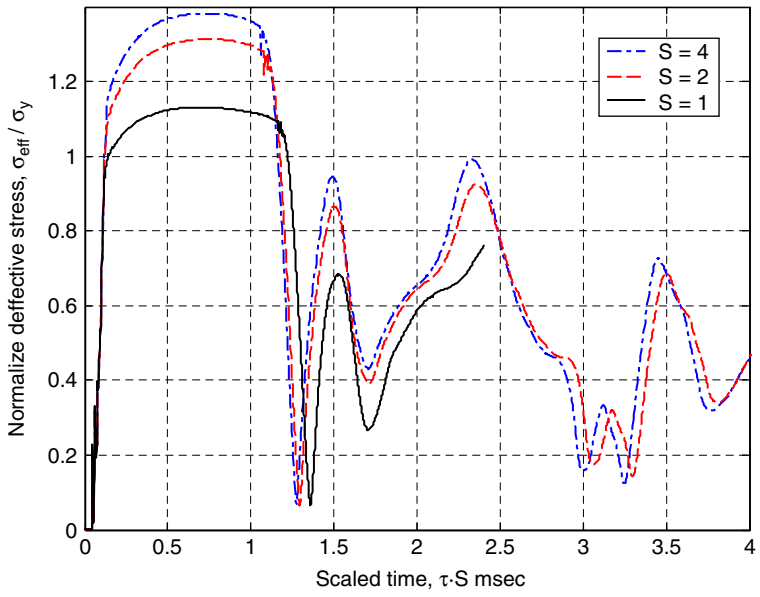

Fig. 13. Normalized effective stress at different scales vs. scaled time (material properties vary with thickness).

time history of the normalized stresses at the midpoint of the plate for the corresponding conditions shown in the last example.

5.2. Experimental results

Experiments were performed at two selected scales, $S = 2$ and 4. Three pairs of cases were compared experimentally. First, a case where the structural response is mostly dynamic elastic, while the second and

Table 2
Experimental and numerical results

S	t (m)	D (m)	W (kg TNT)	R (m)	δ/t Experimental	δ/t Numerical
2	0.02	1	3.75	0.2	2.70	2.62
4	0.01	0.5	0.468	0.1	2.60	2.59
2	0.02	1	8.75	0.2	5.35	5.24
4	0.01	0.5	1.094	0.1	4.85	4.98
2	0.02	1	8.75	0.13	8.25	8.15
4	0.01	0.5	1.094	0.065	7.45	7.72

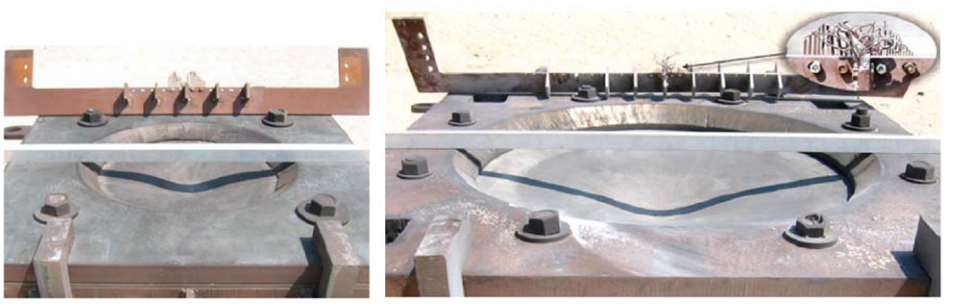

Fig. 14. Experimental result at $S = 4$ (left) and $S = 2$ (right).

third cases treat increasing plastic strains in the structural dynamic response. Table 2 lists the various experimental parameters compared to the numerical predictions of the experiments.

For example, let us select the first case where the model has scale factor $S = 2$, plate thickness $t = 0.02$ m, plate diameter $D = 1$ m, charge weight $W = 3.75$ kg TNT, and the plate distance from center of charge $R = 0.2$ m. This represents a charge of 30 kg TNT for the full scale prototype, where $S = 1$, $t = 0.04$ m, $D = 2$ m, and $R = 0.4$ m. In that case the experimental normalized peak deflection $\delta/t = 2.7$, while the numerical matching parameter $\delta/t = 2.62$. This is equivalent to selecting a scaling factor of $S = 4$ for instance, so that $t = 0.01$ m, $D = 0.5$ m, $W = 0.468$ kg TNT, and $R = 0.1$ m. In that case the corresponding normalized peak deflection remains similar $\delta/t = 2.6$ for the experimental data and match the numerical parameter $\delta/t = 2.59$.

Consider now the third case where large dynamic plastic deformations are achieved. The model has scale factor $S = 2$, plate thickness $t = 0.02$ m, plate diameter $D = 1$ m, charge weight $W = 8.75$ kg TNT (that represents 70 kg TNT for the full scale prototype, $S = 1$), and the plate distance from center of charge $R = 0.13$ m. In that case the experimental normalized peak deflection $\delta/t = 8.25$ while the numerical matching parameter $\delta/t = 8.15$. This is equivalent to selecting a scaling factor of $S = 4$ for instance, so that $t = 0.01$ m, $D = 0.5$ m, $W = 1.094$ kg TNT, and $R = 0.065$ m. In that case the corresponding normalized peak deflection remains similar $\delta/t = 7.45$ for the experimental data and match the numerical parameter $\delta/t = 7.72$. Fig. 14 compares the residual plastic deformations for both scaling factors, $S = 2$ and 4, regarding the third case.

From this table, it appears that the experimental and numerical results are in excellent agreement. It should be noted that, as long the dynamic response is mostly elastic the varying material properties with thickness have no effect on the scaling, as expected. However, when the dynamic deformations are mainly plastic, the scaling is affected, as discussed previously.

6. Discussion

This paper addresses the delicate problem of scaling the dynamic response of circular RHA steel plates to large bare spherical air blast explosions (high explosive without fragmentation, not confined, and

non-localized). The scaling employed here is geometrical (replica) for the structure and based on Hopkinson's law for the explosive charge. While this concept is not new, it has not been previously applied and verified to the specific problem of large charges that are initiated from a close-range.

Three different types of boundary conditions were investigated in the preliminary stage. For each case, a different response was observed, past an initial period. While some similarity was observed between the "free" and "structure" conditions, it was decided to consider further only the "constrained" condition that is more practical from an experimental point of view. In any case, care should be exercised to replicate the actual boundary conditions of the prototype for the scaled problem. One should also keep in mind that the present simulations do not address fracture. If a critical strain or stress is adopted as the failure criterion, its value may well be reached during the inertial phase for which all boundary conditions yield identical results.

Scaling model is affected when the "same" material has different mechanical properties at different scaling factors. Thus, scaling up the results should take into account the effect of the varying mechanical properties with thickness according to the calculated numerical results. Note that the problem treated here is not affected by strain rate sensitivity of the RHA steel. The observed variability is of the order of 5–10% for scaling factor $S = 2$, which should be taken into account for engineering design purposes.

As a final remark, it may seem surprising that plasticity, as a nonlinear phenomenon, scales so well. However, this observation has already been made, e.g. in the work of Rosenberg et al. [25], who studied the geometric scaling of long-rod penetration, and observed that geometrical scaling holds for ductile penetrators and that any deviation from this scaling should be attributed to brittle failure mechanisms at the penetrator's head.

To summarize, the excellent agreement observed between the numerical simulations and the actual explosion experiments provide a powerful engineering tool, when an accurate estimate of the plate's maximal deflection is needed. The scaling down technique employed here is deemed to reduce both the design time and high experimental costs involved in the investigation of these problems.

7. Conclusions

A scaling procedure for the dynamic deformation of constrained steel circular plates subjected to large explosions of spherical charges has been assessed with respect to experimental results. The comparisons indicate very good agreement.

The experimental and numerical results of this investigation show that the structural response of the plate can be efficiently modeled and scaled down using geometrical (replica) together with Hopkinson's (cube root) scaling.

Scaling the actual problem appears to be unaffected by the rate-sensitivity of the RHA steel. However, one should take into account the variability of mechanical properties with plate thickness, with their effect on the normalized peak deflection. Thus, when transforming the scaled model result up to the prototype, the test result should be corrected according to the variability of yield stress with plate thickness used in the numerical calculations.

Acknowledgement

This research was partly supported by Col. Asher Peled Memorial Research (Grant #2005650). The authors would like to thank Dr. David Touati from IMI, Central Laboratory Division, for his support and useful suggestions during the study. Useful discussions with Prof. S.R. Bodner are acknowledged.

References

[1] Nurick GN, Olson MD, Fagnan JR, Levin A. Deformation and tearing of blast-loaded stiffened square plates. Int J Impact Eng 1995;16(2):273–91.

[2] Galiev SU. Experimental observations and discussion of counterintuitive behavior of plates and shallow shells subjected to blast loading. Int J Impact Eng 1996;18(7–8):783–802.

[3] Nurick GN, Gelman ME, Marshall NS. Tearing of blast loaded plates with clamped boundary conditions. Int J Impact Eng 1996;18(7–8):803–27.
[4] Harding JE. Response of stiffened and unstiffened plates subjected to blast loading. Eng Struct 1998;20(12):1079–86.
[5] Rudrapantna NS, Vaziri R, Olson MD. Deformation and failure of blast-loaded square plates. Int J Impact Eng 1999;22:449–67.
[6] Rudrapantna NS, Vaziri R, Olson MD. Deformation and failure of blast-loaded stiffened plates. Int J Impact Eng 2000;24:457–74.
[7] Ramajeyathilagam K, Vendhan CP, Bhujanga VR. Non-linear transient dynamic response of rectangular plates under shock loading. Int J Impact Eng 2000;24:999–1015.
[8] Chung Kim Yuen S, Nurick GN. Experimental and numerical studies on the response of quadrangular stiffened plates. Part I: subjected to uniform blast load. Int J Impact Eng 2005;31:55–83.
[9] Langdon GS, Chung Kim Yuen S, Nurick GN. Experimental and numerical studies on the response of quadrangular stiffened plates. Part II: localised blast loading. Int J Impact Eng 2005;31:85–111.
[10] Menkes SB, Opat HJ. Tearing and shear failure in explosively loaded clamped beams. Exp Mech 1973;13:480–6.
[11] Wen HM, Jones N. Experimental investigation of the scaling laws for metal plates struck by large masses. Int J Impact Eng 1993;13:485–505.
[12] Jacob N, Chung Kim Yuen S, Nurick GN, Bonorchis D, Desai SA, Tait D. Scaling aspects of quadrangular plates subjected to localized blast loads—experiments and predictions. Int J Impact Eng 2004;30:1179–208.
[13] Raftenberg MN. Close-in blast loading of a steel disc—sensitivity to steel strength modeling. Int J Impact Eng 1997;20:651–62.
[14] Hanssen AG, Enstock L, Langseth M. Close-range blast loading of aluminum foam panels. Int J Impact Eng 2002;27:593–618.
[15] Barenblatt GI. Scaling. Cambridge: Cambridge University Press; 2003. p. 37–51.
[16] Jones N. Structural impact. Cambridge: Cambridge University Press; 1989. p. 489–519.
[17] Baker W. Explosions in air. Austin: University of Texas Press; 1973. p. 54–77.
[18] LS-DYNA, Livermore Software Technology Corporation. Lawrence Livermore National Laboratory, Livermore, CA, USA.
[19] Kingerly C, Bulmarsh G. Airblast parameters from TNT spherical air burst and hemispherical surface burst. ARBRL-TR-02555, USArmy Ballistic Research Laboratory, Aberdeen Proving Ground, MD, 1984.
[20] CONWEP, Conventional Weapons Effects, US Army TM-855, 1992.
[21] Johnson GR, Cook WH. A constitutive model and data for metals subjected to large strain, high strain rates and high temperature. In: Proceedings of the 7th International Symposium on Ballistics, The Hague, The Netherlands, 1983. p. 541–8.
[22] Lee E, Finger M, Collins W. JWL equation of state coefficients for high explosives. Rept-UCID-16189, Lawrence Livermore National Laboratory, 1973.
[23] Dobratt BM. LLNL explosive handbook properties of chemical explosives and explosive simulants. Rept-UCRL-52997, Lawrence Livermore National Laboratory, University of California, 1992.
[24] SSAB. Oxelosund, Armox Protection Plate, AM International Specification, Edition 2, 2001.
[25] Rosenberg Z, Kreif R, Dekel E. A note on the geometric scaling of long-rod penetration. Int J Impact Eng 1997;19(3):277–83.